

Role of dispersion on zero-average-index bandgaps

Enrique Silvestre,¹ Ricardo A. Depine,² María L. Martínez-Ricci,² and Juan A. Monsoriu^{3,*}

¹*Departamento de Óptica, Universidad de Valencia, 46100 Burjassot, Spain*

²*Grupo de Electromagnetismo Aplicado, Departamento de Física, Facultad de Ciencias Exactas y Naturales, Universidad de Buenos Aires, Ciudad Universitaria, Pabellón I, C1428EHA Buenos Aires, Argentina*

³*Departamento de Física Aplicada, Universidad Politécnica de Valencia, 46022 Valencia, Spain*

*Corresponding author: jmonsori@fis.upv.es

Received June 24, 2008; revised October 3, 2008; accepted October 22, 2008;
posted November 6, 2008 (Doc. ID 97835); published March 3, 2009

We consider periodic multilayers combining ordinary positive index materials and dispersive metamaterials with negative index in some frequency ranges. These structures can exhibit photonic bandgaps which, in contrast with the usual Bragg gaps, are not based on interference mechanisms. Changing the dispersion models for the constituent metamaterial, we investigate its role in the production of zero-average-index bandgaps. In particular, we show the effect of each constitutive parameter on both bandgap edges. Finally, we give some approximated analytical expressions in terms of average parameters for the determination of the upper and lower limits of the zero-average refractive-index bandgap. © 2009 Optical Society of America

OCIS codes: 160.3918, 230.4170, 260.2110.

1. INTRODUCTION

Photonic crystals (PCs) are artificial composites constituted by periodic arrangements of dielectric materials. These structures, when illuminated with an electromagnetic wave propagating along certain directions, can present ranges of forbidden frequencies called photonic bandgaps (PBGs) [1]. This effect has been observed in both one-, two-, and three-dimensional structures (see [2] and references therein). The simplest one-dimensional (1D) PC is the well known Bragg mirror, a periodic structure consisting of two different alternating layers of conventional dielectric materials [3]. As a result of the scalability of the Maxwell equations (see [2], for instance), multiple interference of Bragg scattering underlying those forbidden bands in the optic regime can appear at any frequency range of the electromagnetic spectrum, and therefore PCs can be designed to manipulate lightwave propagation—from microwaves to X-rays. The broadness of this phenomenon has allowed conceptual transfers between different frequency ranges, with deep implications from both a fundamental and a technological point of view.

Interest in PC microstructures has increased since the appearance of metamaterials (MMs). These are new, artificially constructed composites exhibiting electromagnetic properties that are difficult to achieve with conventional, naturally occurring materials [4,5]. Key representatives of this new class of materials are MMs with a negative index of refraction; such property arises in media with simultaneously negative electric permittivity and magnetic permeability. These artificial materials were proposed by Veselago some decades ago [6], but it was not until recently that they were fabricated for the microwave regime [7,8] and, through a process of miniaturization, they are currently being made to operate in the terahertz regime [9,10]. These composites are usually designed exploiting the resonances of complex metallic inclusions in a homo-

geneous dielectric matrix in such a way that, when illuminated by radiation of wavelength sufficiently greater than a typical distance in the structure, they behave as an effective homogeneous material with negative permittivity and permeability in a certain frequency range.

The inclusion of MMs in PCs has given rise to new kinds of PBGs that do not originate from interference in the periodic structure and are fundamentally different from the above-mentioned Bragg gaps. The first kind of non-Bragg gap appears in multilayers combining ordinary materials (positive refractive index) and MMs with negative refractive index. When the volume-averaged refractive index of the multilayer equals zero, the structure cannot support propagating waves and exhibits a forbidden band [11–13]. A different kind of non-Bragg gap in these multilayered structures emerges as a consequence of material dispersion. When the permittivity or the permeability of the MM vanishes for a certain frequency, another gap can appear around that frequency [14]. Unlike zero-averaged refractive-index gaps, these gaps occur at frequencies where only a single constituent material of the multilayered structure intrinsically shows zero refractive index. Additionally, as shown in [14,15], zero-permeability and zero-permittivity gaps are polarization dependent, very robust against disorder, and they can interact with the zero-averaged refractive-index PBG giving rise to new behaviors. Despite this, dispersion is often ignored when photonic structures are designed.

In this paper we investigate the importance of material dispersion in negative-index media. In particular, we will focus on showing how MM dispersion affects the zero-averaged refractive-index (zero- \bar{n}) bandgap limits. The paper is organized as follows. In Section 2 the main features of the non-Bragg gaps present in PCs with MMs are reviewed. In Section 3 we analyze the dependence of the zero- \bar{n} bandgap limits on MM dispersion. Finally, in Section 4 the more outstanding results are summarized. An

$\exp(-i\omega t)$ time-dependence is implicit throughout the paper, with ω the angular frequency, t the time, and i the imaginary unit.

2. BASIC THEORY

We consider a 1D periodic structure consisting of layers of two different materials: a conventional dielectric with permeability μ_2 , permittivity ϵ_2 and thicknesses d_2 , and a dispersive MM with permeability μ_2 , permittivity ϵ_2 and thicknesses d_2 . The period of the structure is $d=d_1+d_2$. The stratification direction is the y axis, and we consider wave propagation in the x - y plane. Let the function $f(x,y)$ represent the z -directed component of the electric field for the TE-polarization case (electric field parallel to the layers), and the z -directed component of the magnetic field for the TM-polarization case (magnetic field parallel to the layers). The waves in the periodic structure have the form of Bloch modes whose fields satisfy the condition $f(x,y+d)=f(0,y)\exp i(k_x x + Kd)$, where k_x is the wave vector component along the layers and K is the Bloch wave number. In order to obtain the dispersion relation for K we have used the transfer matrix formalism [16]. In it, the half trace of the transfer matrix characterizing the unit cell provides $K(\omega, k_x)$. For two-layered periodic structures, it can be written as follows:

$$\xi \equiv \cos(Kd) = \cos(k_{1y}d_1)\cos(k_{2y}d_2) - \frac{1}{2} \left[\frac{\sigma_2 k_{1y}}{\sigma_1 k_{2y}} + \frac{\sigma_1 k_{2y}}{\sigma_2 k_{1y}} \right] \sin(k_{1y}d_1)\sin(k_{2y}d_2), \quad (1)$$

where the index $j=1,2$ indicates the layer, $\sigma_j=\mu_j$ for TE polarization or $\sigma_j=\epsilon_j$ for TM polarization, $k_{jy}^2=k_j^2-k_x^2$, and $k_j=n_j\omega/c$ are wave numbers in each medium with refractive indexes n_j . The quantity ξ determines the multilayer band structure. It takes real values for lossless media and real k_x . Regimes where $|\xi|<1$ correspond to real K and thus to propagating Bloch waves. In regimes where $|\xi|>1$, K is an imaginary number; therefore the Bloch wave is evanescent, and this regime corresponds to forbidden bands (or gaps) of the periodic medium.

Forbidden bandgaps in the band structure are due to several mechanisms. The usual Bragg forbidden bands of the periodic medium occur under the following conditions [17]:

$$k_{1y}d_1 + k_{2y}d_2 = p\pi, \quad p = \pm 1, \pm 2, \dots, \quad (2a)$$

$$\sigma_2 k_{1y} \neq \sigma_1 k_{2y}, \quad (2b)$$

$$k_{1y}d_1 \neq q\pi, \quad q = 1, 2, \dots \quad (2c)$$

Unusual transmission bands, reported in [17], occur when only conditions (2a) and (2b), but not condition (2c), hold.

MM multilayers can also exhibit non-Bragg gaps. The zero-permeability and zero-permittivity gaps occur at frequencies where a constitutive parameter of the MM— μ_2 for TE polarization or ϵ_2 for TM polarization—changes its sign, and therefore, these gaps do not depend on the multilayer structure [14]. On the other hand, for multilayers comprising both positive- and negative-index dispersive materials, the zero- \bar{n} condition will always be met

for some particular frequency, $\nu_{\bar{n}}$, and another kind of gap arises even if the multilayer is not periodic [18]. In the binary periodic multilayer under consideration, the zero- \bar{n} gap occurs when the conditions

$$k_{1y}d_1 + k_{2y}d_2 = 0, \quad (3a)$$

$$\sigma_2 k_{1y} \neq \sigma_1 k_{2y}, \quad (3b)$$

are simultaneously attained, which is impossible if both layers in the unit cell have either positive or negative refractive index.

It has been observed [13] that, when the frequencies in the zero- \bar{n} gap are smaller than the frequencies at which permeability or permittivity vanish, and for small values of the layer thicknesses d_1 and d_2 , the edges of the zero- \bar{n} gaps correspond to frequencies at which $\xi=+1$ [see Eq. (1)]. These values are determined by the zeros of the following functions [13]:

$$q(\nu) = \sin \frac{d_1 k_{1y}}{2} \cos \frac{d_2 k_{2y}}{2} + \frac{\sigma_2 k_{1y}}{\sigma_1 k_{2y}} \cos \frac{d_1 k_{1y}}{2} \sin \frac{d_2 k_{2y}}{2}, \quad (4a)$$

$$r(\nu) = \sin \frac{d_1 k_{1y}}{2} \cos \frac{d_2 k_{2y}}{2} + \frac{\sigma_1 k_{2y}}{\sigma_2 k_{1y}} \cos \frac{d_1 k_{1y}}{2} \sin \frac{d_2 k_{2y}}{2}, \quad (4b)$$

since $\sin^2(Kd/2) = q(\nu)r(\nu)$ [19].

3. DEPENDENCE OF ZERO- \bar{n} BANDS ON METAMATERIAL DISPERSION

The purpose of this section is to show how dispersion affects the limits of these bandgaps for 1D systems including layers of positive and negative refractive-index materials. To this end, we first analyze a binary system made of alternating layers of air as a positive index material ($\epsilon_1=\mu_1=1$) and dispersive MM with a negative index in some frequency range. Second, we tackle the case of a ternary multilayer.

In order to model the effective constitutive parameters of the MM several expressions have been proposed depending on the metamaterial composition. Different dispersion laws provide different numerical values, but the same behavior for the band edges, as it is shown later. To make clear the role of dispersion on zero- \bar{n} bandgaps, an arbitrary, but dispersive, model can be chosen, being the particular choice for ϵ_2 and μ_2 not relevant. We have assumed, without loss of generality, families of Lorentz-like models based on the following expressions to describe the MM layers [see Eqs. (6) and (9)]:

$$\hat{\epsilon}(\nu) = 1 - \frac{1.62^2}{\nu^2 - 0.95^2}, \quad (5a)$$

$$\hat{\mu}(\nu) = 1 - \frac{3^2}{\nu^2 - 0.902^2}, \quad (5b)$$

where the frequency, $\nu=\omega/(2\pi)$, is given in gigahertz [see Fig. 1(a)]. Figure 1 also shows the projected band struc-

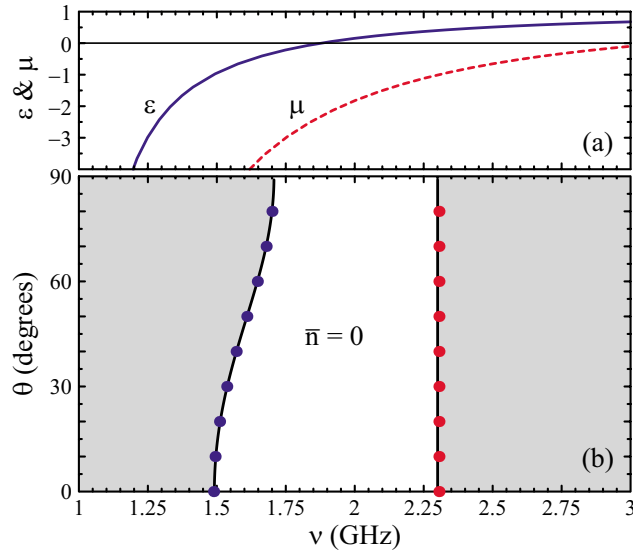


Fig. 1. (Color online) (a) Frequency dependence of the effective parameters μ_2 and ϵ_2 , as given by Eqs. (5). Note that ϵ_2 and μ_2 become zero at different frequency values [$\nu_\epsilon=1.878$ GHz and $\nu_\mu=3.133$ GHz (out of the plot range)]. (b) Projected band structure for TE polarization and different angles of incidence corresponding to periodic stacks with air layers ($\epsilon_1=\mu_1=1$) and MM layers [ϵ_2 and μ_2 shown in (a)], both of the same width ($d_1=d_2=6$ mm). Dots represent the low-frequency limit of the zero- \bar{n} bandgap edges given by Eqs. (7).

ture for TE polarization and angles of incidence ranging from 0 to 90° of periodic stacks with air layers and MM layers. The widths of both layers are $d_1=d_2=6$ mm for all the binary multilayers analyzed. In Fig. 1(b), the white region indicates a band where propagation is forbidden in the crystal regardless of K , the Bloch wave number. It includes the frequencies at which conditions (3) are satisfied, i.e., it is a zero- \bar{n} gap. At these particular frequencies that allow us to label the gap ($\nu_{\bar{n}}=1.707$ GHz at normal incidence), both constitutive parameters of the MM are negative, although the gap can also spread over regions where both are not.

The spectral response of MMs is often simplified assuming that one of the parameters, or even both, is non-dispersive. In the latter case, the zero- \bar{n} bandgap covers all the electromagnetic spectrum if $\mu_2(\nu)=\hat{\mu}(\nu_{\bar{n}})$ and $\epsilon_2(\nu)=\hat{\epsilon}(\nu_{\bar{n}})$ [11] or it can disappear if the zero- \bar{n} condition is not satisfied. Moreover, our analysis shows that the process through which this bandgap arises is more complex than expected and that the two constitutive parameters do not act in the same way over the gap limits. In fact, in Fig. 2 we can see that each bandgap limit is ruled, at normal incidence, by one of the constitutive parameters. If we just make the magnetic permeability constant, $\mu_2(\nu)=\hat{\mu}(\nu_{\bar{n}})$, and the dielectric permittivity dispersive, $\epsilon_2(\nu)=\hat{\epsilon}(\nu)$, we can see that a forbidden band has only a lower limit [Fig. 2(a)]. On the contrary, if we just make the dielectric permittivity constant, $\epsilon_2(\nu)=\hat{\epsilon}(\nu_{\bar{n}})$, and the magnetic permeability dispersive, $\mu_2(\nu)=\hat{\mu}(\nu)$, the band extends from $\nu\approx 0$ up to an upper limit [Fig. 2(c)]. It is worth mentioning that these limits match closely with those obtained when both constitutive parameters are considered frequency dependent [Fig. 2(b)].

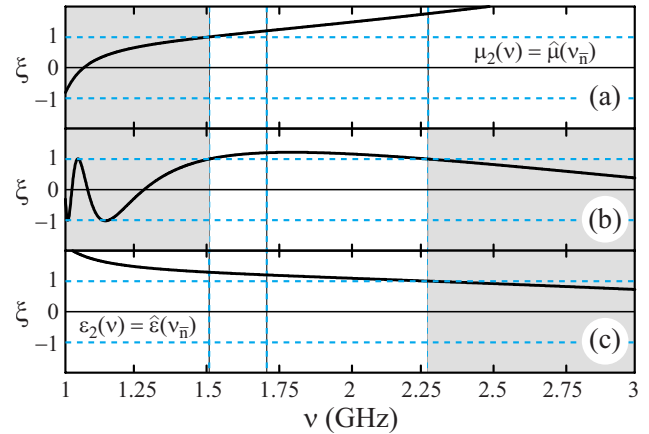


Fig. 2. (Color online) Half of the trace of the unit cell translation matrix, ξ , as given by Eq. (1), for the structure considered in Fig. 1, at normal incidence, when either ϵ_2 (a), or μ_2 (c), or both (b) are considered dispersive.

To shed light on the widening process of the zero- \bar{n} gap, we have parametrized the dispersion relations around $\nu_{\bar{n}}$ as follows:

$$\epsilon_2(\nu; \alpha_\epsilon) = \hat{\epsilon}(\nu_{\bar{n}}) + \alpha_\epsilon [\hat{\epsilon}(\nu) - \hat{\epsilon}(\nu_{\bar{n}})], \quad (6a)$$

$$\mu_2(\nu; \alpha_\mu) = \hat{\mu}(\nu_{\bar{n}}) + \alpha_\mu [\hat{\mu}(\nu) - \hat{\mu}(\nu_{\bar{n}})], \quad (6b)$$

where α_ϵ and α_μ are real numbers. In this way, we cover a broad range of dispersions: if $\alpha_\epsilon=\alpha_\mu=1$, Eqs. (5) are recovered, and diminishing α_ϵ or α_μ , this parametrization allows us to reduce the dispersion of the corresponding constitutive parameter and thus to follow the gap limits evolution. In the limit, when α_ϵ or α_μ are zero, a nondispersive model is considered (see insets in Fig. 3).

The evolution of the bandgap limits with dispersion for TE polarization and two different angles of incidence is shown in Fig. 3. When the slope of $\mu_2(\nu)$ is the only one

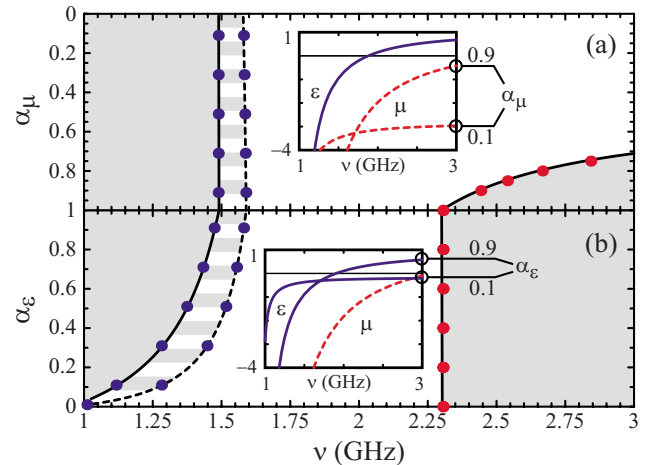


Fig. 3. (Color online) Evolution of the zero- \bar{n} bandgap when the constitutive parameters, $\mu_2(\nu)$ and $\epsilon_2(\nu)$, change their slope around $\nu_{\bar{n}}$ [see Eqs. (6)] for TE polarization and two different angles of incidence (solid curves, 0°; dashed curves, 45°; dots, band edge low-frequency limits). (a) $\alpha_\epsilon=1$ and α_μ ranging from 1 to 0. (b) $\alpha_\mu=1$ and α_ϵ ranging from 1 to 0. The gray- and white-striped zone is forbidden for one angle of incidence and allowed for the other one. This insets show the dispersion relations for two cases close to the limits of the considered ranges.

reduced, by changing α_μ from 1 to 0 and fixing $\alpha_\epsilon=1$, the upper limit of the bandgap increases, whereas the lower limit remains constant [see Fig. 3(a)]. On the contrary, when α_ϵ is reduced from 1 to 0 and α_μ is maintained equal to 1 (and therefore only $\epsilon_2(\nu)$ is made less dispersive) the lower limit of the bandgap diminishes [Fig. 3(b)]. In other words, as it could be expected, the less dispersive are the constitutive parameters, the wider is the zero- \bar{n} bandgap, and, in addition, the bandgap limits seem to depend separately on each of these parameters.

The dependence of the zero- \bar{n} band edges on all the parameters can be better understood after calculating the low frequency limit ($d_1 k_{1y} \ll 1$ and $d_2 k_{2y} \ll 1$) of the equations $q(\nu)=0$ and $r(\nu)=0$. These limits turn out to be

$$\bar{\mu} = 0, \quad (7a)$$

$$(\omega/c)^2 \bar{\epsilon} + k_x^2 \bar{\mu}^{-1} = 0, \quad (7b)$$

for TE polarization, and

$$\bar{\epsilon} = 0, \quad (8a)$$

$$(\omega/c)^2 \bar{\mu} + k_x^2 \bar{\epsilon}^{-1} = 0, \quad (8b)$$

for TM polarization, where $\bar{\epsilon}$, $\bar{\mu}$, $\bar{\epsilon}^{-1}$, and $\bar{\mu}^{-1}$ are the volume average of the dielectric permittivity, the magnetic permeability, and their inverses, respectively. We have found that this low frequency limit provides very good estimates for the zero- \bar{n} bandgap edges. In Fig. 3, the relative error of the proposed approximation is about or smaller than 1%. It is worth noticing that the dependence of the zero- \bar{n} bandgap edges on the actual dispersion profile of the material constitutive parameters comes, in the previous equations, through the four mentioned volume averages.

On the other hand, Fig. 3 shows that the zero- \bar{n} bandgap edges have a well-defined dependence on each constitutive parameter, the upper edge being ruled by μ and the lower edge by ϵ . However, it has been evaluated for TE polarization considering the case in which $\epsilon_2(\nu_{\bar{n}}) > \mu_2(\nu_{\bar{n}})$. To study the opposite case, $\epsilon_2(\nu_{\bar{n}}) < \mu_2(\nu_{\bar{n}})$, we introduce the following expressions for the constitutive parameters, again based on Eqs. (5),

$$\epsilon_2(\nu; \Delta\epsilon) = \hat{\epsilon}(\nu) + \Delta\epsilon, \quad (9a)$$

$$\mu_2(\nu; \Delta\mu) = \hat{\mu}(\nu) + \Delta\mu, \quad (9b)$$

where $\Delta\epsilon$ and $\Delta\mu$ are linked in such a way that $\nu_{\bar{n}}$, the frequency at which $\bar{n}=0$, remains constant (see the inset in Fig. 4).

Figure 4 shows the evolution of the zero- \bar{n} bandgap edges when $\Delta\mu$ changes from 0 to 3, both at normal and oblique incidence (0° and 45°), and for TE polarization. It can be observed that when the transverse impedances of both materials are matched $k_{1y}/\sigma_1 = k_{2y}/\sigma_2$ [see Eq. (3b)], the zero- \bar{n} gap vanishes. At this point, both Eqs. (7) are simultaneously satisfied and, correspondingly, the zero- \bar{n} condition is also fulfilled at the same frequency.

Again, the low frequency limit given by Eqs. (7) provides good estimates for the zero- \bar{n} bandgap edges. For the results in Fig. 4, the relative error of this approxima-

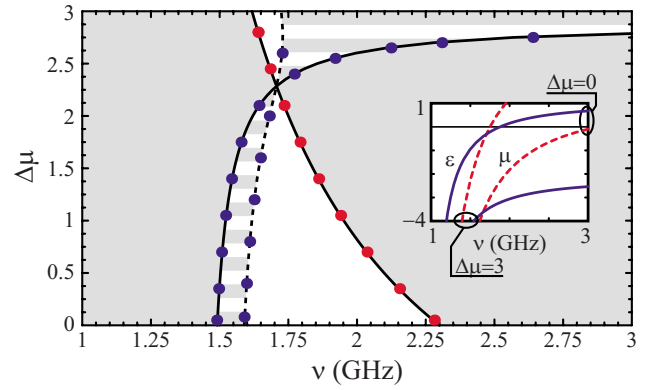


Fig. 4. (Color online) Evolution of the zero- \bar{n} gap as a function of $\Delta\mu$ [see Eq. (9)] for TE polarization and two different angles of incidence (solid lines, 0° ; dashed lines, 45° ; dots, band edge low-frequency limits). At $\Delta\mu=2.28$, when the transverse impedance matching between both materials is achieved, the zero- \bar{n} gap vanishes. Gray- and white-striped zones are forbidden for one angle of incidence and allowed for the other one. The inset shows the dispersion relations for the two cases in the limits of the considered range.

tion is smaller than 1%, except at normal incidence near the region where the bandgap edge becomes nearly flat, where the relative error grows up to 2%. It is interesting to note that, in the case under consideration, the point at which both bandgap edges cross does not depend on the angle of incidence, since under these conditions $\bar{\sigma}^{-1}$ is also equal to zero (as $\bar{\sigma}=0$ and $d_1=d_2$).

In the previous numerical examples, nonlossy MMs have been chosen for simplicity. However, Eqs. (7) and (8) are also valid when losses are considered. In this case, the bandgap edges are given by the real part of their complex roots. By way of example we analyze stacks of 30 periods of the multilayer considered in Fig. 1(b) when dissipation is included through a damping constant γ :

$$\epsilon_2(\nu; \gamma) = 1 - \frac{1.62^2}{\nu^2 - 0.95^2 + i\gamma\nu}, \quad (10a)$$

$$\mu_2(\nu; \gamma) = 1 - \frac{3^2}{\nu^2 - 0.90^2 + i\gamma\nu}. \quad (10b)$$

Figures 5 show the reflectance spectra for TE polarization, different angles of incidence, and two values of γ .

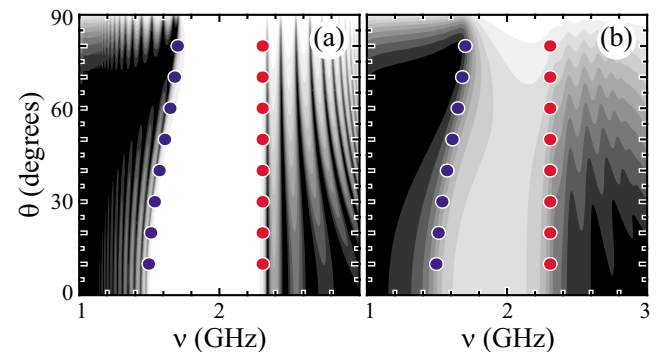


Fig. 5. (Color online) Reflectance spectra of two stacks of 30 periods of the multilayer analyzed in Fig. 1(b) when a lossy MM is considered: (a) $\gamma=0.01$ GHz and (b) $\gamma=0.1$ GHz. The polarization is TE and the angle of incidence ranges from 0 to 90° .

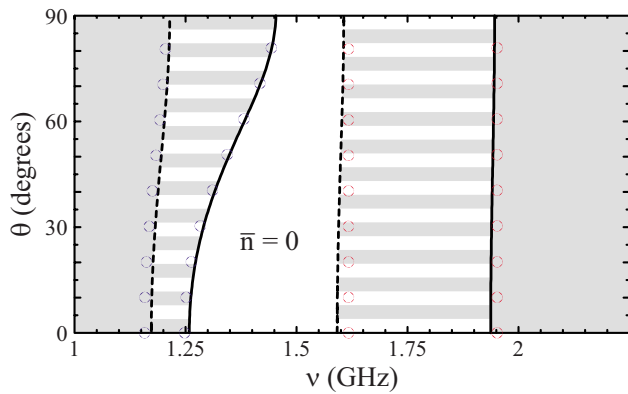


Fig. 6. (Color online) Projected band structure for TE polarization and different angles of incidence corresponding to two periodic stacks with layers made of air ($\epsilon_1 = \mu_1 = 1$), a dispersive MM [$\epsilon_2(\nu) = \hat{\epsilon}(\nu)$, and $\mu_2(\nu) = \hat{\mu}(\nu)$], and two different high-index dielectrics with (a) $\epsilon_3 = 4$ and $\mu_3 = 3$ (solid lines) and (b) $\epsilon_3 = 4$ and $\mu_3 = 3$ (dashed lines), the three of them of the same width ($d_1 = d_2 = d_3 = 6$ mm). In both cases, dots represent the low-frequency limit of the zero- \bar{n} bandgap edges given by Eqs. (7). Gray- and white-striped zones are forbidden for one case and allowed for the other one.

Even for a value as high as 0.1 GHz, Eqs. (7) provide good estimates for the band edges.

To conclude this section, it is worth mentioning that the analytical approximate expressions obtained for the zero- \bar{n} bandgap edges of binary multilayers [Eqs. (7) and (8)] can be applied to other kinds of periodic multilayers. This can be guessed from the fact that those expressions are written in terms of factors that do not depend explicitly on any detail of the multilayer structure, but only on the ϵ , μ , ϵ^{-1} , and μ^{-1} averages. To investigate the validity of this prediction, we show in Fig. 6 the projected band structure, for TE polarization and angles of incidence ranging from 0 to 90°, of two different ternary periodic stacks for which Eqs. (4) for $q(\nu)$ and $r(\nu)$ do not hold. These ternary stacks are made of the same dispersive MM [$\epsilon_2(\nu) = \hat{\epsilon}(\nu)$ and $\mu_2(\nu) = \hat{\mu}(\nu)$], and two positive-index materials ($\epsilon_1 = \mu_1 = 1$, $\epsilon_3 = 2$, and $\mu_3 = 2$ for the first case, and $\epsilon_3 = 4$ and $\mu_3 = 3$ for the second one). The three layers have the same width ($d_1 = d_2 = d_3 = 6$ mm). Again, but now for nonbinary multilayers, Eqs. (7) provide good estimates for the zero- \bar{n} bandgap edges, the relative error being smaller than 1.5%.

4. CONCLUSION

We have studied the role of dispersion on MM multilayers exhibiting zero-average-index bandgaps. Our analysis highlights the important role played by the unavoidable (and usually strong) dispersive character of MMs, a point that usually plays a secondary role or is even neglected.

By using Lorentz-like models to describe the MM layers, we have shown the effect of each constitutive parameter on each of the bandgap edges. In order to gain some physical insight on the complex dependency of these bandgaps on the constitutive and geometrical parameters of the multilayer, we have obtained some analytical approximate expressions—in terms of average parameters—for the bandgap edges. These expressions are the low-frequency limit of the analytical counterparts

for a binary multilayer, and they are also valid when lossy MMs are considered. However, the numerical examples illustrate that those approximated limits provide very good agreement even in the case of nonbinary periodic multilayers. Since those expressions are written in terms of factors that do not depend explicitly on any detail of the multilayer structure, we could expect their validity in more general situations.

ACKNOWLEDGMENTS

This work was funded by the Ministerio de Educación y Ciencia, Spain and FEDER (grants TEC2005–07336–C02–02/MIC and PCI2005–A7–0255). It was also financially supported by Consejo Nacional de Investigaciones Científicas y Técnicas (CONICET), Universidad de Buenos Aires (UBA) and Agencia Nacional de Promoción Científica y Tecnológica (PICT-11-1785), Argentina. R.A.D. acknowledges support from Secretaría de Estado de Universidades e Investigación (fellowship SAB2006–0074), Spain for a sabbatical stay at the University of Valencia, and he is gratefully indebted to the kind hospitality of Pedro Andrés and his coworkers.

REFERENCES

1. E. Yablonovitch, “Photonic band-gap structures,” *J. Opt. Soc. Am. B* **10**, 283–295 (1993).
2. J. D. Joannopoulos, R. D. Meade, and J. N. Winn, *Photonic Crystals: Molding the Flow of Light* (Princeton U. Press, 1995).
3. Y. Fink, J. Winn, S. Fan, C. Chen, J. Michel, J. Joannopoulos, and E. Thomas, “A dielectric omnidirectional reflector,” *Science* **282**, 1679–1682 (1998).
4. D. Smith, J. Pendry, and M. Wiltshire, “Metamaterials and negative refractive index,” *Science* **305**, 788–792 (2004).
5. N. Engheta and R. W. Ziolkowski (eds.), *Metamaterials: Physics and Engineering Explorations* (Wiley-IEEE, 2006).
6. V. G. Veselago, “The electrodynamics of substances with simultaneously negative values of permittivity and permeability,” *Sov. Phys. Usp.* **10**, 509–514 (1968).
7. J. B. Pendry, A. J. Holden, D. J. Robbins, and W. J. Stewart, “Magnetism from conductors and enhanced nonlinear phenomena,” *IEEE Trans. Microwave Theory Tech.* **47**, 2075–2084 (1999).
8. D. R. Smith, W. J. Padilla, D. C. Vier, S. C. Nemat-Nasser, and S. Schultz, “Composite medium with simultaneously negative permeability and permittivity,” *Phys. Rev. Lett.* **84**, 4184–4187 (2000).
9. G. Dolling, M. Wegener, C. M. Soukoulis, and S. Linden, “Negative-index metamaterial at 780 nm wavelength,” *Opt. Lett.* **32**, 53–55 (2007).
10. V. M. Shalaev, “Optical negative-index metamaterials,” *Nat. Photonics* **1**, 41–48 (2007).
11. J. Li, L. Zhou, C. T. Chan, and P. Sheng, “Photonic bandgap from a stack of positive and negative index materials,” *Phys. Rev. Lett.* **90**, 083901 (2003).
12. N. Panoiu, R. Osgood, S. Zhang, and S. Brueck, “Zero-n bandgap in photonic crystal superlattices,” *J. Opt. Soc. Am. B* **23**, 506–513 (2006).
13. M. de Dios-Leyva and O. E. González-Vásquez, “Band structure and associated electromagnetic fields in one-dimensional photonic crystals with left-handed materials,” *Phys. Rev. B* **77**, 125102 (2008).
14. R. A. Depine, M. L. Martínez-Ricci, J. A. Monsoriu, E. Silvestre, and P. Andrés, “Zero permeability and zero permittivity bandgaps in 1D metamaterial photonic crystals,” *Phys. Lett. A* **364**, 352–355 (2007).

15. J. A. Monsoriu, R. A. Depine, M. L. Martínez-Ricci, and E. Silvestre, "Interaction between non-Bragg bandgaps in 1D metamaterial photonic crystals," *Opt. Express* **14**, 12958–12967 (2006).
16. P. Yeh, A. Yariv, and C. Hong, "Electromagnetic propagation in periodic stratified media. I. General theory," *J. Opt. Soc. Am.* **67**, 423–438 (1977).
17. L. Wu, S. He, and L. Chen, "On unusual narrow transmission bands for a multilayered periodic structure containing left-handed materials," *Opt. Express* **11**, 1283–1290 (2003).
18. J. A. Monsoriu, R. A. Depine, and E. Silvestre, "Non-Bragg bandgaps in 1D metamaterial aperiodic multilayers," *J. Eur. Opt. Soc. Rapid Publ.* **2**, 07002 (2007).
19. M. de Dios-Leyva, J. Sabin, and J. López-Gondar, "Band and branch inversion phenomena in GaAs-Al_xGa_{1-x}As superlattices," *Phys. Status Solidi B* **134**, 615–620 (1986).